J Digit Imaging (2018) 31:210–223
DOI 10.1007/s10278-017-9992-3

Can Laws Be a Potential PET Image Texture Analysis Approach for Evaluation of Tumor Heterogeneity and Histopathological Characteristics in NSCLC?

Seyhan Karacavus[1,2] · Bülent Yılmaz[3] · Arzu Tasdemir[4] · Ömer Kayaaltı[5] · Eser Kaya[6] · Semra İçer[2] · Oguzhan Ayyıldız[3]

Published online: 6 July 2017

Abstract We investigated the association between the textural features obtained from ^{18}F-FDG images, metabolic parameters (SUVmax, SUVmean, MTV, TLG), and tumor histopathological characteristics (stage and Ki-67 proliferation index) in non-small cell lung cancer (NSCLC). The FDG-PET images of 67 patients with NSCLC were evaluated. MATLAB technical computing language was employed in the extraction of 137 features by using first order statistics (FOS), gray-level co-occurrence matrix (GLCM), gray-level run length matrix (GLRLM), and Laws' texture filters. Textural features and metabolic parameters were statistically analyzed in terms of good discrimination power between tumor stages, and selected features/parameters were used in the automatic classification by *k*-nearest neighbors (*k*-NN) and support vector machines (SVM). We showed that one textural feature (gray-level nonuniformity, GLN) obtained using GLRLM approach and nine textural features using Laws' approach were successful in discriminating all tumor stages, unlike metabolic parameters. There were significant correlations between Ki-67 index and some of the textural features computed using Laws' method (r = 0.6, p = 0.013). In terms of automatic classification of tumor stage, the accuracy was approximately 84% with *k*-NN classifier (k = 3) and SVM, using selected five features. Texture analysis of FDG-PET images has a potential to be an objective tool to assess tumor histopathological characteristics. The textural features obtained using Laws' approach could be useful in the discrimination of tumor stage.

Keywords Texture analysis · PET · Tumor heterogeneity · Tumor histopathological characteristics · Ki-67

✉ Seyhan Karacavus
seyhan.karacavus@sbu.edu.tr

Bülent Yılmaz
bulent.yilmaz@agu.edu.tr

Arzu Tasdemir
atasdemir@erciyes.edu.tr

Ömer Kayaaltı
kayaalti@erciyes.edu.tr

Eser Kaya
kaya_eser@yahoo.com

Semra İçer
ksemra@erciyes.edu.tr

Oguzhan Ayyıldız
ayyildizned@gmail.com

[1] Department of Nuclear Medicine, Saglık Bilimleri University, Kayseri Training and Research Hospital, 38010 Kayseri, Turkey

[2] Department of Biomedical Engineering, Erciyes University, Engineering Faculty, Kayseri, Turkey

[3] Department of Electrical and Electronics Engineering, Abdullah Gül University, Engineering Faculty, Kayseri, Turkey

[4] Department of Pathology, Saglik Bilimleri University, Kayseri Training and Research Hospital, Kayseri, Turkey

[5] Department of Computer Technologies, Erciyes University, Develi Hüseyin Şahin Vocational College, Kayseri, Turkey

[6] Department of Nuclear Medicine, Acibadem University, School of Medicine, İstanbul, Turkey

Introduction

Positron emission tomography (PET) is a useful functional imaging technique whose effectiveness to stage or restage tumors, evaluate tumor response to treatment, define patient prognosis, and guide surgery and radiotherapy for patients with cancers of non-small cell lung cancer (NSCLC) is proven [1, 2]. Exact tumor stage evaluation is important to plan therapy protocol accurately and to prevent unnecessary surgery. The uptake of ^{18}F-FDG used extensively in PET studies is closely related to the parameters determining the biological behavior of the lesion such as in healthy, tumorous, and inflammatory cells, growth index, tissue blood supply, and hypoxia [3]. These tumor characteristics can affect the degree and heterogeneity of tumor FDG uptake and semi-quantitative parameters, such as standard uptake value (SUV), total lesion glycolysis (TLG), and metabolic tumor volume (MTV) [4]. In addition, these parameters are mostly histogram based and have the shortcomings of histogram analysis. Histogram-based parameters cannot describe the gross texture coming from relationships of two or more voxels [5]. On the other hand, it is a well-known fact that the characterization of the lesion using excisional or fine-needle biopsy, considered as the golden standard, might have sampling error, which would not represent the actual biological behavior and the intra-tumoral heterogeneity. Therefore, a more meaningful feature of the tumor uptake from PET images for the determination of intra-tumoral heterogeneity has recently been investigated intensively.

The field of radiomics proposes the extraction of additional features from different data coming from various imaging modalities. We know that medical images contain more valuable information than may be obtained by visual analysis. In this context, texture features noninvasively extracted from PET images may allow us to characterize the histopathological tumor properties in vivo at molecular level. In this kind of studies, including ours, the goal is to find one or more biomarker/s (feature/s) carrying predictive and prognostic information.

Owing to the increase in PET scanners' spatial resolution, there has been a tendency among researchers towards using image processing tools/approaches on PET images recently. Among these are image texture analysis methods, which can assess radiotracer uptake that reflects the image heterogeneity, and in turn, biological heterogeneity of the underlying tumor [6–8] relatively accurately. Texture analysis includes a set of pattern analysis approaches that quantify the interrelationship of the pixels or voxels via different mathematical methods. The parameters derived from texture analysis have been found to be useful in better lesion characterization, image segmentation, monitoring and predicting of therapy response, and prognosis [9–12]. In this context, numerous texture parameters have been proposed so far. However, to give a general sense of some of these parameters, in a certain region of interest (ROI) on the medical image (especially PET images here), lower uniformity, higher entropy, higher standard deviation, lower skewness, and higher kurtosis computed using the pixel distribution represent increased heterogeneity. Nevertheless, the relationship between these textural parameters and commonly used semi-quantitative parameters and tumor stage, type, and histopathological features has not been fully defined or explored in NSCLC.

When we scan the literature, we obverse that (i) in some studies, researchers included only a small number of patients ($n <= 20$) in their analysis [13, 14] and some other studies used patients from different cancer types but did not focus on a NSCLC group, and therefore, few number of NSCLC patients were examined [8, 9]; (ii) most studies used only a few texture analysis methods and thus extracted limited number of texture parameters [15]; and (iii) there are only a few studies that considered using textural parameters for automatic classification of tumor stage or subtype [16, 17].

In this study, we investigated the relationship between the textural features obtained from ^{18}F-FDG images and other metabolic parameters (SUVmax, SUVmean, MTV, TLG), and tumor histopathological characteristics (stage and Ki-67 proliferation index), and whether these textural features could be used in the automatic discrimination/classification of tumor stage in NSCLC. In addition, an important contribution of this study is to introduce a texture analysis approach, called Laws' texture filter, in the intra-tumoral heterogeneity quantification for NSCLC. Here, the superiority of this technique compared to the approaches reported in the PET texture analysis literature is presented in terms of correlation with metabolic parameters, tumor stage, proliferation index, and automatic classification.

Our and many other groups' goal in this kind of research is to find more robust features indicating the heterogeneity of the lesion extracted from the PET images that could be used in malignancy analysis, stage discrimination (especially difficult to stage cases), subtype determination, prognosis, and therapy response monitoring. It would be very beneficial to perform these analyses using a noninvasive approach like texture analysis. In recent years, this has been a hot topic of research in medical image analysis that has the potential to pave new ways in the noninvasive characterization of the tumors.

Methods

Patient Population

In this retrospective study, 83 patients with non-small cell lung cancer (NSCLC) that previously underwent ^{18}F-FDG-PET/CT imaging for cancer staging before surgery, chemotherapy, or radiotherapy treatment according to the stage of their disease from March 2010 to April 2014 were evaluated in the

Acıbadem Kayseri Hospital. Malignant disease was confirmed by histopathological verification in all patients. Patients were grouped as stage I, II, III, or IV, using conventional CT criteria for tumor size and local invasion and PET assessments of nodal and distant metastases by well-trained imaging specialists according to the seventh edition of the American Joint Committee on Cancer (AJCC) TNM classification guidelines [18]. In patients without histopathological T-stage, N-stage, or M-stage verification, clinical follow-up served as the standard of reference for T, N, and M stages. Ten patients were excluded because their tumors were conglomerating with regional lymph nodes and/or conjugating inflammatory lesions. In addition, six patients with a tumor volume smaller than 5 ml were not included in this study, because the number of voxels was not sufficient to obtain a robust statistic as suggested by [19]. The remaining 67 patients consisted of 8 females and 59 males, with a mean age of 62.4 ± 8.7, were evaluated in this study. In order to balance the group sizes, patients with stages I and II were combined to form one group, giving a total of three groups (stages I and II, stage III, and stage IV). The number of patients with TNM stage I–II, III, or IV was 27, 19, and 21, respectively. The tumor subtypes were also balanced (45% adenocardinomas—ADCs and 55% squamous carcionomas—SqCCs). Patient characteristics are presented in Table 1. In addition, immunohistochemical examination was performed by the pathology expert in our team on a subgroup containing 40 of all patients, because samples were not available for the rest of the group, i.e., for remaining 27 patients. This study was approved by the research ethics committee of the Kayseri Research and Training Hospital. All procedures performed in studies involving human participants were in accordance with the ethical standards of the institutional and/or national research committee and with the 1964 Helsinki Declaration and its later amendments or comparable ethical standards. Informed consent was obtained from all individual participants included in the study.

Table 1 Clinical and demographical characteristics and metabolic parameters of all patients (n = 67)

Clinical features	
Age	62.4 ± 8.7
Gender (F/M)	8/59
Tumor type	
Adenocarcinoma	30
Squamous cell carcinoma	37
TNM stage	
I	7
II	20
III	19
IV	21
PET semi-quantitative values	
SUVmax	16.1 ± 8.3
SUVmean	8.9 ± 4.5
MTV	47.9 ± 39.2
TLG	463.7 ± 435.4

SUV standardized uptake value, *MTV* metabolic tumor volume, *TLG* total lesion glycolysis

PET/CT Study

Images were acquired at the Acıbadem Hospital Nuclear Medicine Department, Kayseri, Turkey, using a PET/CT scanner (Siemens Biograph 6, Hi-Rez). The scanner had energy resolution less than 15%, lutetium oxyorthosilicate (LSO) detector, 98-mm^3 volumetric resolution, 4.3-mm spatial resolution (Hi-Rez property), and high-quality imaging capability and 6-slice multi-detector CT system.

Ten to fifteen millicuries (370–555 MBq) of ^{18}F-FDG was intravenously injected to the patients whose blood glucose level was below 150 mg/dl. The PET/CT acquisitions were performed 60.4 ± 4.2 min after the injection in the supine position between the head and the femur. First, CT and, then in the same range at eight or nine bed positions (2–3 min at each position), PET scanning were carried out for all patients. After the reconstruction of the acquired images using 3D iterative reconstruction algorithm, two nuclear medicine experts assessed the 3D whole body projection (maximum intensity projection, MIP) and the coronal, sagittal, and transverse cross-sections visually and semi-quantitatively using the e-Soft software platform (Siemens, USA). The regions of interest (ROIs) on the target lesions were determined semiautomatically, starting with the expert's initial rectangular area selection followed by the scanner's built-in software. The mean SUV (SUVmean), maximum SUV (SUVmax), metabolic tumor volume (MTV), and total lesion glycolysis (TLG) values were computed using the same platform (Fig. 1). The MTV and TLG values were computed using the approach described by Larson et al. [20]. TLG was computed by the multiplication of the MTV and SUVmean values. For patients with multiple lesions, TLG was obtained by the summation of TLG values computed from each lesion.

Histopathological Examination

The pathological specimens were acquired using excisional or fine-needle biopsy. The immunohistochemical (IHC) staining was performed on the 5-μm-thick sections cut from the tissue blocks, which were composed of formalin-fixed, paraffin-embedded specimens from all available materials. IHC staining was examined by using of avidin-biotin-peroxidase method. The 5-μm sections were prepared for investigating the Ki-67 expression (Thermo Scientific Ki-67, Rabbit Monoclonal Antibody). The Ki-67 expression was assessed by obtaining the labeling index (LI positive epithelial cells/100 epithelial

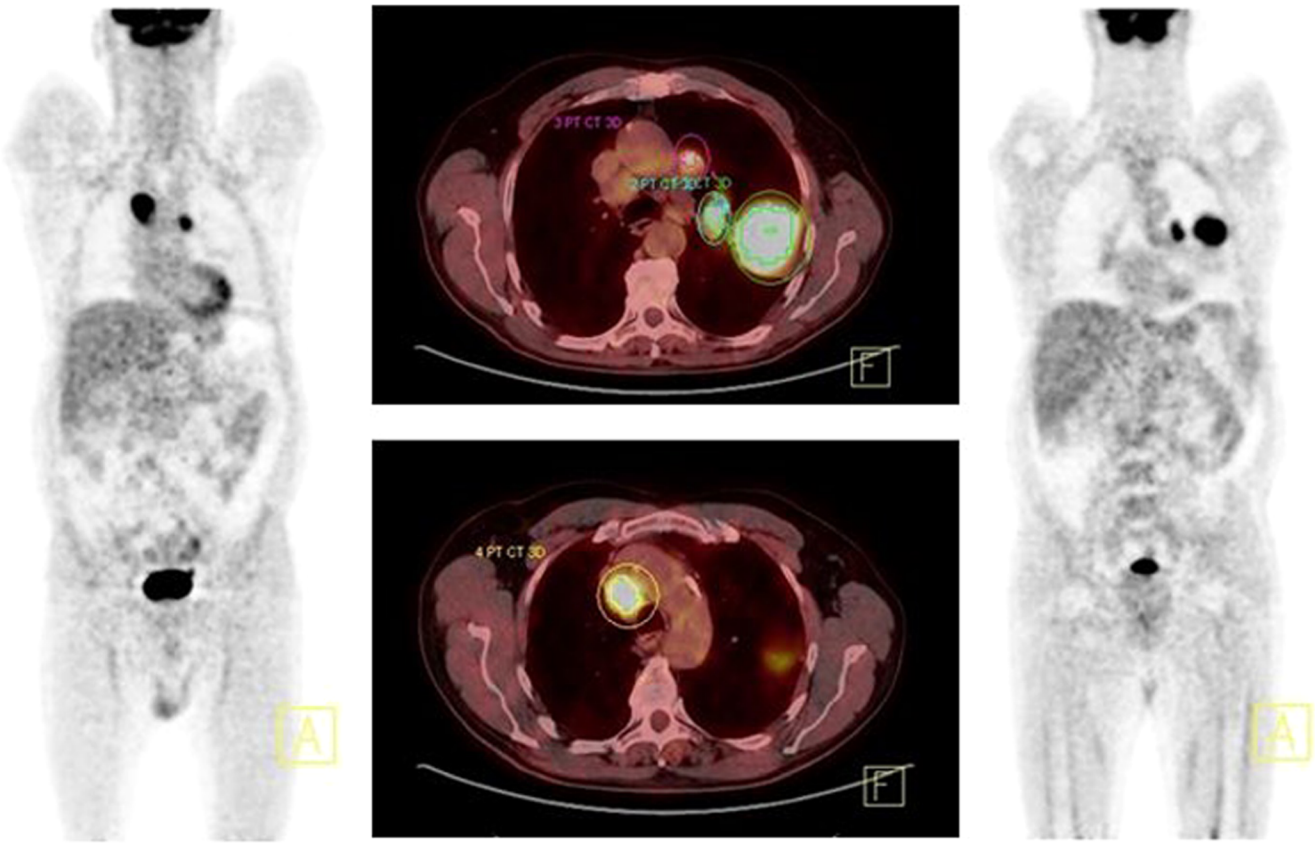

Fig. 1 Regions of interest on PET/CT images for the MTV and TLG computations on a patient

cells) for each section. Ki-67 immunohistochemistry study was performed in a subgroup of 40 patients out of all 67 patients. The nuclear staining was considered as positive for Ki-67. IHC staining was performed using an automated system (Autostainer Leica Bond-max, Leica Microsystems, Bannockburn, IL, USA). For Ki-67, the most intense area that has the nuclear staining in the tumor tissue was examined. The Ki-67 score as the percentage of tumor cells was graded as follows by an expert pathologist with a 6-year experience score (+) for 10–29%, score (++) for 30–49%, and score (+++) for 50–100%.

Image Processing

PET/CT images and acquisition details were saved as DICOM image files. The PET/CT slices that contained tumor lesions were evaluated using the graphical user interface of the acquisition system in fused and separate modes. The slice with the highest SUVmax value in the ROI of the target lesion was determined. When the adjacent FDG-avid lesions or structures (inflammation, lymph nodes, etc.) could not be identified, the case was excluded from the study. The screenshot of this slice from the monitor of the workstation has been saved as a reference for further analysis.

The image processing steps were performed using MATLAB (MathWorks, MA, USA) technical computing environment based on those selected/specific PET slices (one slice for each subject). The processing steps were as follows: (i) tumor segmentation, (ii) binning, and (iii) texture analysis (Fig. 2). Before the segmentation step, a rectangular region that contained the target lesion on the associated PET slice was visually selected with the help of the nuclear medicine expert in our research team (SK), as the initial ROI, to work on. On this region, a popular segmentation approach called Otsu's method [21] was used to distinguish the background from the tumor. Otsu's method is used to perform clustering-based image thresholding or the binarization of an image. This method involves iterating through all the possible threshold values and calculating a measure of spread (intra-class variance) for the pixels that fall either in foreground or in background. The algorithm assumes that the image contains bi-modal histogram then calculates the optimum threshold separating those two classes so that their combined intra-class variance is minimal. Otsu's segmentation approach was previously used in segmentation of brain magnetic resonance images [22], cerebrovascular segmentation [23], nuclei extraction [24], and small animal PET/CT [25].

In the binning step, for an efficient texture analysis, the pixel values on the segmented region that contains the tumor

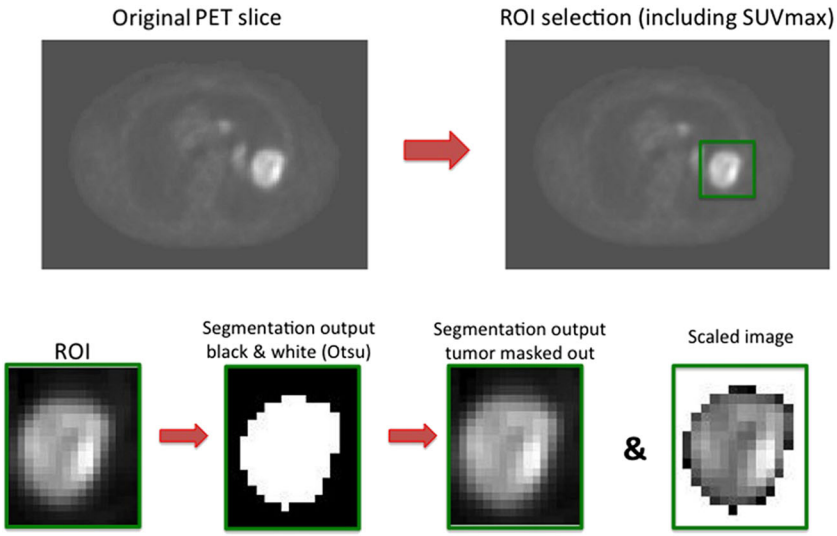

Fig. 2 ROI selection and segmentation steps shown on a tumor located on the left lung

were scaled. The binning is done in such way that the wide range of intensity values was linearly mapped to be between 1 and 64. Different binning levels like 16, 32, 64, and 128 were tested, and it is found that 64 was the optimal value in terms of resolution and computational time. As Clausi [26] has shown, more than 64 levels do not improve classification accuracy and levels less than 24 can produce unreliable results.

Texture Analysis

The final step involved performing texture analysis on the binned regions with tumors. A total of 137 features were extracted using first order statistics [27] (FOS, 7 features) and three different texture analysis approaches. The texture analysis approaches were the gray-level co-occurrence matrix (GLCM, 21 features), gray-level run length matrix (GLRLM, 11 features), and the Laws' texture features (Laws, 98 features) [27–30].

In the FOS, the properties were extracted from the segmented tumor (i.e., not binned), which did not take the neighboring pixel values into account. In this approach, from the pixel intensity values, $I(x,y)$, a histogram depicting the ratio of the number of pixels with a certain gray level to the total number of pixels in the region was formed. Using the pixel intensity values and the histogram features, whose definitions were given in [27], shown in Table 2, the features were computed.

The second feature extraction approach used was the GLCM, which describes the relationship between the neighbor pixels and depicts the occurrence rate of the brightness levels on the image at fixed distances and orientations. GLCMs were computed for 0, 45, 90, and 135° with 1-pixel distance. All the features mentioned below were computed and averaged over these four angles in order to make them rotationally invariant. In this approach, scaled ROIs were used in order to describe or characterize the relationship between the neighbors in a standardized manner. For further details on GLCM computation, we refer the reader to [28]. The final GLCM gives the probabilities of co-occurrences, which is then used in the derivation of texture features (see Table 2). The definitions of these features are given in [31]. In our case, the binning was performed to make final images of 64 gray levels and the final (normalized) GLCMs were 64 × 64 matrices.

The third feature extraction approach was the GLRLM. The term *gray level run* in the GLRLM approach means the sequential pixels with the same gray level in the same direction. GLRLM is a 2D matrix and each element shows how many times the gray level i runs in length of j in the angle direction occurred [29]. When the number of neighbor pixels that have the same gray level is low, the texture has a fast variation. The most common 11 GLRLM features were proposed by Galloway [29], Chu et al. [32], and Dasarathy and Holder [33]. All the features shown in Table 2 were computed and averaged over 0, 45, 90, and 135° in order to make them rotationally invariant. The angles used in the GLCM and GLRLM computation are commonly used for 2D image texture analysis.

The last texture analysis approach we used was the Laws' texture features. To our knowledge, the feasibility/performance of this approach has not been investigated in the PET image analysis area until now. It has been used on ultrasound images of the fatty liver [34], on high-resolution digital radiographs of the bones [35], and on CT images of the lungs [36].

In this approach, local masks or filters are employed in detecting various types of textures. In order to generate these local masks, one-dimensional kernels known as "Level (L), Edge (E), Spot (S), Wave (W), and Ripple (R)" are convolved [30] to produce two-dimensional (2D) 5 × 5 kernels. L gives a

Table 2 Texture features and metabolic parameters according to TNM stage of all patients

Tumor Stage	I–II	III	IV
Texture features			
FOS			
Energy	5.26 ± 4,69[a,b]	6.34 ± 5.11[a]	7.81 ± 5.43[b]
Entropy	−3.74 ± 3.93[a,b]	−5.08 ± 3.52[a]	−7.39 ± 6.79[b]
Std	2.86 ± 2.42[b]	2.57 ± 1.42	2.27 ± 1.23[b]
Mad	2.45 ± 2.11[b]	2.11 ± 1.23	1.92 ± 1.02[b]
GLCM			
Contrast	206.79 ± 82.91[a,b]	157.97 ± 69.71[a]	133.577 ± 76.73[b]
Coenergy	0.16 ± 0.04[a]	0.19 ± 0.03	0.18 ± 0.03
Homogeneity	0.025 ± 0.014[a,b]	0.012 ± 0.006[a]	0.014 ± 0.007[b]
Autocorre	0.485 ± 0.195[a]	0.620 ± 0.138	0.578 ± 0.144
Cluspromi	0.082 ± 0.037[a]	0.109 ± 0.033	0.101 ± 0.032
Maxprobap	11.539 ± 2.643[a]	9.031 ± 1.973	9.906 ± 2.352
Sumosquare	3.877 ± 0.551[a,b]	4.533 ± 0.433[a]	4.447 ± 0.624[b]
Sumaverage	0.037 ± 0.016[a,b]	0.024 ± 0.009[a]	0.025 ± 0.014[b]
Difentropy	3.033 ± 0.486[a,b]	3.554 ± 0.332[a]	3.349 ± 0.479[b]
Infcorr1	0.0012 ± 0.0003[a,b]	0.0009 ± 0.0002[a]	0.0008 ± 0.0001[b]
Infcorr2	2.585 ± 0.262[a,b]	2.764 ± 0.132[a]	2.785 ± 0.144[b]
Invdifnor	−0.752 ± 0.59[a,b]	−0.664 ± 0.574[a]	−0.673 ± 0.091[b]
Homogemat	0.857 ± 0.027[a]	0.884 ± 0.022	0.874 ± 0.026
Corrematv	0.955 ± 0.017[a]	0.970 ± 0.011	0.965 ± 0.014
GLRLM			
GLN	1.97 ± 0.37[c]	2.56 ± 0.61[c]	3.33 ± 1.21[c]
RLN	56.04 ± 19.04[a,b]	86.11 ± 23.41[a]	108.58 ± 49.29[b]
LGRE	0.057 ± 0.022[b]	0.043 ± 0.014	0.042 ± 0.025[b]
SRLGE	0.055 ± 0.021[b]	0.042 ± 0.014	0.041 ± 0.024[b]
LRLGE	0.062 ± 0.026[b]	0.047 ± 0.016	0.045 ± 0.027[b]
Laws[c,d] (entropy)			
E5L5	21.75 ± 4.73	29.21 ± 6.04	36.57 ± 2.67
S5L5	12.73 ± 1.87	16.82 ± 3.79	22.38 ± 8.74
R5L5	10.61 ± 3.17	15.14 ± 4.64	21.38 ± 9.49
W5E5	4.03 ± 1.09	5.37 ± 1.37	7.39 ± 2.77
R5E5	4.71 ± 1.45	6.61 ± 1.83	9.13 ± 3.96
W5S5	2.27 ± 0.78	3.21 ± 0.87	4.63 ± 1.97
R5W5	3.14 ± 1.06	4.71 ± 1.97	6.86 ± 3.23
E5E5	8.89 ± 1.64	11.07 ± 2.44	13.97 ± 4.44
S5S5	2.21 ± 0.95	3.37 ± 1.02	4.87 ± 2.31
Metabolic parameters			
SUVmax	17.8 ± 10.8	14.9 ± 5.1	14.8 ± 6.6
SUVmean	9.6 ± 5.4	9.4 ± 3.5	7.5 ± 4.1
MTV	50.6 ± 47.3[a,b]	44.5 ± 33.1[a]	47.9 ± 41.5[b]
TLG	490 ± 439[a,b]	399.8 ± 343[a]	499 ± 435[b]

[a] Statistically significant difference between TNM stages I–II with stage III ($p < 0.05$)

[b] Statistically significant difference between TNM stages I–II with stage IV ($p < 0.05$)

[c] Statistically significant difference between TNM stages of all groups from each other ($p < 0.05$)

[d] 48 out of 98 features computed using Laws' approach were able to discriminate at least two stages. The list here only depicts the ones that were successful in discriminating three stages together.

center-weighted local average, E responds to row or column step edges, S detects spots, and R detects ripples. In our case, the lengths of L, E, S, W, and R kernels were 5. For instance, L and E are convolved to produce L5E5 filter, Wave and Ripple are convolved to produce W5R5 filter, and so on (please refer to Table 2 for all filters). These filters are later used in determining the strength or energy of different types of textures. Once a filter is applied to the image, resultant filtered image is further processed by windowing, offset, and normalization operations [35]. Here, each pixel in the filtered image is replaced with a normalized texture energy measure (TEM) at that pixel, yielding a new image that is referred to as the TEM_NR image. In our application, direction of texture features was not important; therefore, we have combined TEM_NR images, which were obtained to detect texture features at different orientations, into a single rotationally invariant texture energy measurement/image by averaging them (Fig. 3). After these steps, 14 final "texture energy images" corresponding to different texture features were obtained, and 7 FOS figures were calculated from each of these texture energy image. Hence, a total of 14 × 7 = 98 Laws' texture features were obtained and used in the statistical analysis and classification part of our study.

It is important to note that all the features (metabolic parameters and the ones computed with different texture analysis approaches) were normalized to be between 0 and 1 for pattern classification phase of the study.

Statistical Analysis

Statistical analysis was performed using SPSS 18.0 software package (IBM, Armonk, New York, USA). Parameters were depicted as mean ± standard deviation. The inter-variance differences were evaluated by Student's *t* test for normally distributed parameters. When more than two groups were compared, ANOVA test and, in the assessment of differences between groups, post hoc Tukey test [37] were employed. For the parameters that had significant difference in tumor stages, error bar graphs were used.

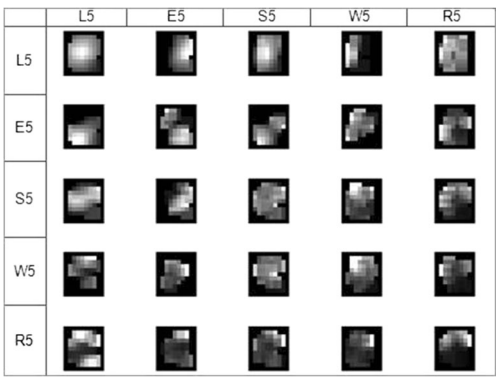

Fig. 3 Illustration of an example organized in a matrix form for Laws' filters applied on a tumor

The correlation between the parameters obtained from the texture analysis and the PET/CT quantitative parameters and the clinical stage and histopathological data was analyzed using Pearson (for continuous variables) and Spearman (for categorical variables) correlation tests. Correlation coefficient was depicted as *r* and the statistical significance level was selected as $p < 0.05$. The aim of the correlation analysis was to determine parameter/s that can discriminate all three tumor stages.

Automatic Classification of Tumor Stages

When there are many parameters or features influencing the outcome, it may be a better idea to resort to the techniques of pattern classification, which can handle/analyze the contributions of all parameters at once. For instance, in our case, we have over 100 texture features generated using automated image analysis. Instead of working with these features or parameters one-by-one, we can design a classifier and quickly and efficiently see and assess the classification or discriminating power in these features for identifying different classes, TNM stage, or tumor subtype in our case. This is the motivation behind using the classification approach in this context. Further, when there are many stages, using features separately may lead to the problem multiple testing [38].

One of the aims of our study was to analyze the feasibility of using pattern classification approaches for the discrimination of three tumor stages (stages I–II, stage III, and stage IV) with the help of textural features and other metabolic parameters like SUVmax, SUVmean, MTV, and TLG.

The classification method we chose was the *k*-nearest neighbors (*k*-NN) approach [39], which is a commonly known and simple to use approach. We have also investigated the usage of support vector machines (SVM) for this data set [40], and the results showed that *k*-NN performed at least as good as SVM although it is a highly simple approach.

In *k*-NN, the samples were multi-dimensional feature vectors each with a tumor stage or subtype label. In the classification phase, a feature vector coming from one ROI was assigned to the class that was most frequently encountered among the *k*-nearest samples ($k = 3$, we have tested $k = 5$ or 7 and found $k = 3$ to be the best choice for this problem), using a proper distance metric such as Euclidean distance. Once a training dataset is formed, a test feature vector is classified by assigning it to the class of the most frequently seen neighbors among the *k* training samples nearest to that vector (if there is a tie, then a random assignment is made among the tying groups). In the testing phase, the samples are randomly divided into three approximately equal and balanced (in terms of containing enough number samples from each class) subsets. Then, each subset is excluded from the complete set and employed as the test set. The remaining samples are used

as the training set. This is repeated over three subsets and the resultant classification performance values is averaged to produce an overall prediction accuracy rate, which is known as the "3-fold cross-validation (CV)" accuracy rate [41]. The confusion matrices are also generated in order to visualize and evaluate classification performance/results in some detail.

In SVM [40], the training samples (features coming from texture analysis approaches) are labeled as a member of one of two (or more) categories/classes. A model, which is a non-probabilistic binary linear classifier, assigns new samples into one class or the other. This model is a depiction of the samples as points in space, mapped so that the samples of the different classes are separated by a well-defined gap that is as wide as possible. Finally, new samples are projected on that same space and estimated to go to a class according to the side of the gap they fall on. In addition, kernels, which map the input parameters into high-dimensional feature spaces, can also be used to perform a non-linear classification. In the classification of part our study, there were three TNM stage classes or two tumor subtype classes. SVM one versus one and one versus all methods were executed with the Gaussian radial basis function kernel. For the SVM applications, the built-in functions available in MATLAB called "fitcsvm" and "predict." The c and gamma values were not optimized for simplicity and used as one. Same as above, a threefold cross-validation was performed.

One of the important steps employed in the classification procedure is called the feature selection in which the best subset representing the original feature set is chosen. For instance, in our study, only 5 out of 137 features were selected to be used in the classification phase. We used sequential forward selection (SFS) method as it is easy to implement and offers reasonable performance [42]. In this method, the "selected features set" is initiated with an empty set and the feature yielding the highest accuracy in the classification of tumor stages is added to the "selected features set." Then, other/remaining features are sequentially included in the selected feature set (now has two features) and the combination/set of features yielding the highest performance becomes the new selected features set and so on. This is continued until five features are gathered or selected. We have observed that typically after five features, the performance did not increase.

Another study to compare the classification performance of each texture parameter family (FOS, GLCM, GLRLM, or Laws) was executed for tumor stage discrimination. In that final study, the SFS method was employed to select five features not from all available parameters but only from each texture parameter family separately. The accuracy, sensitivity, and specificity values for each classification method and each texture parameter family were computed and compared.

Results

Relationship Between Textural or Metabolic Features/Parameters and Tumor Stage

The analysis of variance (ANOVA) and post hoc Tukey test were used to determine the histogram (FOS) and textural (GLCM, GLRLM, and Laws) features and metabolic (SUVmax, SUVmean, MTV, and TLG) parameters that perform best in the discrimination of tumor stages (I–II, III, and IV). The comparisons were made for each parameter (total of 141 parameters, 137 texture plus 4 metabolic parameters) separately.

The results of the statistical analysis showed that one textural feature (GLN) obtained using GLRLM approach and nine textural features (entropy values of E5L5, S5L5, R5L5, W5E5, R5E5, W5S5, R5W5, E5E5, and S5S5) using Laws' approach were successful in discriminating all three TNM stages. As indicated in Table 2, there were some other textural features that yielded statistically significant differences between stages I–II and III, and stages I-II and IV, but not between stages III and IV. Figure 4a, b demonstrates two examples of textural parameters (GLN from GLRLM and entropy of E5L5 from Laws' approaches) that were successful in discriminating against all three stages. Error bars correspond to 95% confidence intervals.

In contrast to the performance of textural features, the metabolic parameters did not show any potential in discriminating all TNM stages. There was no statistically significant difference between the means of SUVmax or SUVmean values in different stages. On the other hand, the means of MTV and TLG parameters were significantly different between stage I–II and III or IV, but not between stages III and IV.

In addition, there was a good correlation between the TNM stage and some textural features such as GLN feature ($r = 0.606$ and $p < 0.001$) coming from GLRLM, and the entropy value of L5E5 ($r = 0.724$ and $p < 0.001$) coming from Laws with the highest r values. On the other hand, although a significant correlation was not observed between FOS, GLCM, GLRLM, and Laws with SUVmax, some textural parameters showed a significant correlation with SUVmean, MTV, and TLG. Table 3 summarizes the correlation analysis results.

Automatic Classification of Tumor Stages

In this part of the study, we used pattern recognition approaches for automatic classification of tumor stages. Along these lines, the classification accuracy, sensitivity, and specificity values were given in Table 4 for k-NN approach and SVM approach with one versus one (OvsO) and one versus all (OvsA) paradigms.

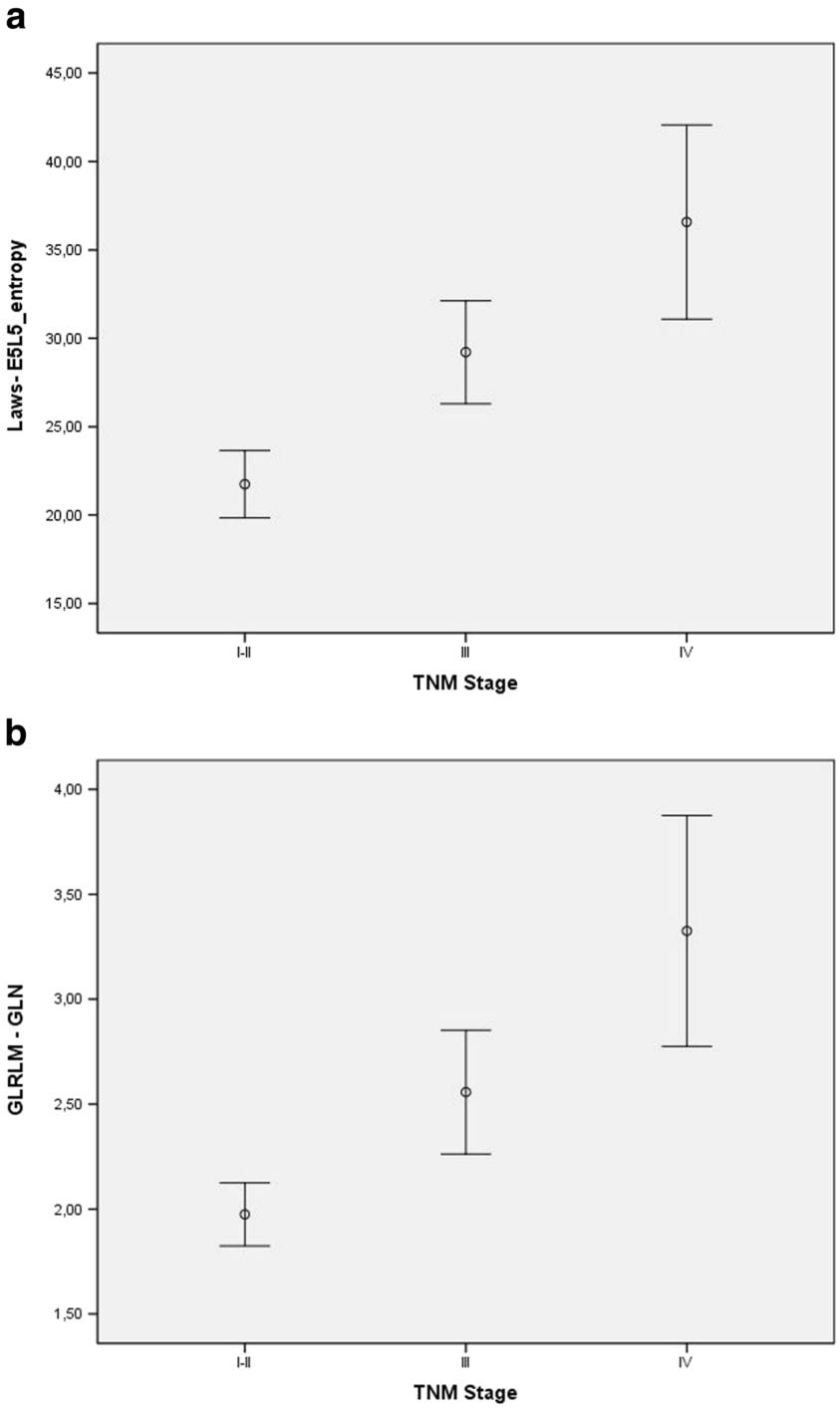

Fig. 4 **a**, **b** Two SPSS plots of textural parameters (GLN and E5L5_entropy from Laws) all three stages

Approximately 84% accuracy with *k*-NN classifier ($k = 3$), 82% OvsO, and 81% OvsA, using five features, were selected with the SFS method (Table 4 all row). The *k*-NN classifier also gave the best sensitivity and specificity values, 93 and 91%, respectively. The increase in the number of features included in the classification phase beyond five did not improve the classification accuracy significantly. According to our investigation, this value was optimal for this study. In this part of the study, again, one textural feature (LRLGE) computed using GLRLM and four features (means of W5S5, R5W5, S5L5, and the skewness of S5S5) coming from Laws' approach were found to be the five best features in the classification of three TNM stages. It is important to note that none of the metabolic parameters were selected by our algorithm to be one of the best features/parameters. This underlines the importance of the texture parameters and the benefits of texture-based image analysis in classifying TNM stage automatically.

Table 3 The highest correlations values obtained between textural features, metabolic parameters, and TNM stages

	TNM	FOS	GLCM	GLRLM	Laws
TNM	1	−0.343 (0.005)	0.428 (<0.001)	0.606 (<0.001)	0.724 (<0.001)
SUVmax	−0.099 (0.428)	−0.152 (0.204)	0.017 (0.893)	−0.044 (0.727)	−0.008 (0.949)
SUVmean	−0.129 (0.303)	−0.287 (0.019)*	0.324 (0.008)*	−0.337 (0.006)*	−0.245 (0.047)*
MTV	0.386 (0.001)	−0.515 (0.001)*	−0.611 (<0.001)*	0.606 (<0.001)*	0.684 (<0.001)*
TLG	0.337 (0.006)	−0.497 (0.001)*	−0.477 (<0.001)*	−0.548 (<0.001)*	−0.641 (<0.001)*

*$p < 0.005$ or $p < 0.001$ statistical significance levels

When we compared the texture parameter families, it was observed that Laws' approach outperformed other texture analysis approaches quite significantly. The accuracy level was around 84% for five selected Laws' features and 65% for five selected features from other families.

Correlations Between Textural or Metabolic Parameters and Histopathological Characteristics

In the 40-patient subgroup, the textural features obtained using Laws' approach such as skewness of E5E5, entropy of S5S5, energy of R5R5, mean of R5S5, mean absolute deviations of W5S5, and E5E5 were correlated with Ki-67 (maximum level was $r = -0.606$ and $p = 0.013$). There were no correlation between FOS, GLCM, and GLRM features and TNM stage with Ki-67. On the other hand, only TLG among metabolic parameters was correlated with Ki-67 ($r = 0.558$ and $p = 0.025$).

Discussion

The ^{18}F-FDG-PET is an imaging technique commonly used to study cellular metabolism in oncology. FDG is a glucose analogue that is trapped by cells [43]. Tumor cells typically show augmented glucose metabolism and thus an increased FDG uptake compared to healthy cells. This characteristic helps the imaging of tumor cells by using PET [44]. In digital PET images, pixels have gray-level intensity values that represent the metabolic rate of glucose corresponding those particular locations/tissues in space [45].

Table 4 The confusion matrix for the automatic classification of TNM stages

		Predicted stage		
		I–II	III	IV
Actual stage	I–II	24	1	2
	III	2	14	3
	IV	1	2	18

Previous studies have explored the potential use of texture analysis in ultrasonography, computed tomography, and magnetic resonance imaging, and reported results supporting the idea that texture features obtained from these images can differentiate the tissue types [46–48]. In contrast to its abundant use and reasonably good performance in such anatomical imaging settings, usage of texture analysis in PET images has progressed relatively slowly, as PET images have relatively poorer spatial resolution compared to anatomical images. In recent years, there has been an increased effort to demonstrate the feasibility of texture analysis on PET images, for the evaluation of tumor heterogeneity [49]. The findings of limited number of studies in the literature [6, 11] and our results reveal that certain textural features have more predictive and prognostic power compared to metabolic parameters such as SUVmax or SUVmean.

Some textural features in NSCLC PET images have already been described/used in the literature. For example, Cook et al. evaluated PET textural features in NSCLC and their relationship with response and survival after chemoradiotherapy [10]. Recently, van Gómez et al. assessed the correlation between the texture features like energy, entropy, contrast, correlation, and homogeneity of FDG-PET images, with metabolic parameters like SUVmax, SUVmean, MTV, and TLG, and pathologic staging in 38 NSCLC patients [50]. Furthermore, Orlhac et al. investigated the correlations between 5 first order statistics and 31 features derived using gray-level co-occurrence matrix, gray-level run length matrix, neighborhood gray-level different matrix, and gray-level zone length matrix approaches [8]. Furthermore, in a recent study, texture features of ^{18}F-FDG uptake heterogeneity in NSCLC were compared with visual assessment performed by two experts showing a moderate correlation between visual scoring results and some texture features [8]. These studies showed that textural features derived from PET images might bring an additional insight into tumor biological behavior.

A more recent review article authored by Sollini et al. provides a comprehensive review of literature describing the state

of the art of FDG-PET/CT texture analysis in NSCLC [51]. The authors cited 85 studies and summarized them in a table that included the effect of segmentation method on tumor volume estimation, comparison of different discretization methods for textural features, sensitivity of texture features to tumor motion, variability of PET textural features using different reconstruction methods, iteration numbers, and voxel size, features for tumor staging, prognosis, and survival. This most recent review showed that the number of studies investigating the use of Laws' features obtained from PET images of NSCLC patients is highly limited. There is only one study [52] in which Laws' features were used to predict the distant metastases.

In this study, our principal aim was to perform a comprehensive investigation on the textural features and metabolic parameters in terms of their correlation, potential in the automatic classification of TNM stages. In addition, we have also demonstrated the feasibility and superior performance of Laws' texture features in this context. We may argue that some textural parameters can serve as a better indicator for tumor stage when compared to metabolic parameters. For example, a textural parameter (entropy of E5L5) can go high as the stage becomes worse. Currently, a further study on the prognostic value of certain textural parameters with a large patient database is pursued in our laboratory.

Our study comprised of images from 67 NSCLC patients, which was one of the most inclusive among the studies published until now. The pairwise correlations were calculated between 141 textural features obtained from ^{18}F-FDG-PET images using four different approaches (FOS, GLCM, GLRLM, and Laws' methods) and metabolic parameters like SUVmax, SUVmean, MTV, and TLG. The Laws' approach was used in the correlation and classification context for the first time for the analysis of PET images and has shown better tumor classification/staging performance compared to other (relatively more popular) texture feature extraction methods. In addition, the correlations between textural features/metabolic parameters and Ki-67 proliferation index and the tumor stage were explored.

It is important to note that none of the metabolic parameters (SUV, MTV, and TLG) could discriminate all three stages at the same time. However, ten texture features were found to be successful in this respect (Table 2). In addition, as the tumor stage increased, the means of all these texture features corresponding to the heterogeneity also increased. The means of SUVmax and SUVmean decreased as the stage increased. This might be due to tissue differentiation or degeneration/deterioration.

One critical finding in our study is that certain Laws' features have a significant potential in the discrimination of TNM stages. Similarly, Laws' features were correlated better with TNM stages when compared to other metabolic parameters and texture features. Furthermore, four Laws' features were selected to the five most effective parameters set in the automatic classification of TNM stages.

In the classification part of the study, we used two classification approaches, namely *k*-NN and SVM, along with a simple feature selection method, namely sequential forward selection. Here, our aim was to demonstrate the feasibility of using such pattern classification approaches that can scrutinize predictive value of many features simultaneously.

Furthermore, Soussan et al. found in their study on invasive breast cancer that Ki-67 (percentage of positive cells) was correlated only with SUVmax and not with textural features [16]. In contrast to this study, for NSCLC, we found a relationship between Ki-67 and certain Laws' features and TLG. TLG has been proposed as a reliable marker of the viable tumor volume, which combines the functional and anatomical information of FDG-PET. Ki-67 is commonly used as a biomarker to determine proliferation of tumor cells and is associated with poorer prognosis. Vessele et al. claimed that FDG-PET might be used to evaluate NSCLC proliferation noninvasively, which might help identifying fast growing NSCLCs with poor prognosis, a potential beneficiary for preoperative chemotherapy [53]. They showed that Ki-67 expression was correlated strongly with FDG uptake ($r = 0.73$; $p < 0.0001$).

Finally, we should note here that there are some limitations associated with the textural features based on analysis and assessment of tumors on PET images: (i) Explaining each textural feature with a specific physiologic process inside the tumor is a daunting task; (ii) due to the low spatial resolution of PET, small tumors cannot be evaluated properly using these features; and (iii) in many studies, the tumor with the largest cross-sectional area is assessed rather than the whole tumor volume. Another limitation of the study is that we obtained the metabolic parameters like MTV and TLG by the summation of all values computed from each lesion (primary tumor and lymph nodes). This is actually how the evaluation of tumor stage and prognosis is performed in clinical practice. However, we have performed the textural analysis only on the primary lesions in order to analyze/determine the stage of the tumor.

In addition to the limitations of the textural features, there are several limitations related to the other steps of the analysis of PET images such as segmentation and classification. For the segmentation of tumors, the researchers have been investigating the use of various approaches: semiautomatic and automatic. Semiautomatic approaches require the selection of an initial region of interest, which is subjective. Automatic approaches may converge to other bright areas on the image such as the heart. Each approach may result in different results, which might affect the computed textural features. The effect of different segmentation approaches on the textural features and classification accuracy has not been investigated in a systematic manner until now. As a group, currently, we are conducting a research on this issue.

However, the absence of a ground truth is the main limitation in this part of the study. The performances of the segmentation step can only be compared with the experts' manual delineation, which is assumed to be the ground truth. In the context of the limitations of the automatic classification of tumor stages, several other approaches might have been added to the study such as linear or quadrature discriminant analysis and neural networks. We preferred using one simple (*k*-NN) and one relative advanced (SVM) approach. The limitations of *k*-NN approach are the followings: (i) There is a need to determine the value of *k*, which might affect the performance. Usually, trial and error is used to optimize that value; (ii) distance type is critical and it is a subjective issue to choose which type is the best for a particular study; and finally, (iii) the computation cost of this approach is high. The limitations of SVM are the followings: (i) The theory covers the determination of the parameters for a given value of the regularization, kernel parameters, and choice of kernel; (ii) kernel models can be sensitive to over-fitting the model selection criterion [54]; and (iii) the computation cost of optimization of RBF parameters may be high. For general limitations of the field radiomics, readers can refer to [55] for a comprehensive review.

Currently, a further study on the prognostic value of certain textural parameters computed from three-dimensional (3D) tumor volumes with a large patient database is pursued in our laboratory. Because the lesions are 3D structures, the 3D texture analysis is more desirable to represent the characteristics of the lesion for a better prognosis and assessment of the treatment response. In addition, the 3D textural analysis can show a stronger association between metabolic parameters and histopathological characteristics.

Even though the number of subjects included in our study is comparable to the other studies performed in this area, we consider that more comprehensive studies, multi-center studies for instance, which will involve relatively large number of subjects will follow our study in the very near future. We believe that the findings of these upcoming studies will further establish reliability and reproducibility of our findings, i.e., the relevance and importance of texture analysis (especially using Laws' features) in evaluating tumors in PET images.

As an outcome of this study, we suggest that along with the parameters employed routinely in the clinic, semiautomatic FDG-PET texture feature extraction/analysis approaches may also be included as a module in image visualization and analysis software(s). In addition, these features may shed light on and improve the understanding of biological behavior of tumors. Furthermore, we believe that the use of texture features in the objective evaluation of the PET images has a strong potential in determining the TNM stage and tumor histopathological characteristics. We anticipate that future studies will also include the quantification of the therapy response and prognosis potentially useful for patient stratification and management, using the methods that we have introduced in this study.

Conclusions

Textural features might reflect the biologic abnormalities that underlie disease and have the potential to be used as a new tool to assess tumor metabolism, stage, and histopathological features in clinical practice in addition to SUVmax, TLG, and MTV. We found that the textural features obtained using Laws' approach could be useful in the discrimination of tumor stage. Laws' features were also correlated with Ki-67 proliferation index.

ADC, adenocardinoma; AJCC, American Joint Committee on Cancer; FDG-PET, ^{18}F-fluorodeoxyglucose-positron emission tomography; FOS, first order statistics; GLCM, gray-level co-occurrence matrix; GLRLM, gray-level run length matrix; IHC, immunohistochemical; MTV, metabolic tumor volume; NSCLC, non-small cell lung cancer; SqCC, squamous carcionoma; SUVmax, maximum and mean standardized uptake value; SUVmean, mean standardized uptake value; TLG, total lesion glycolysis

Acknowledgements This study was funded by TUBITAK (The Scientific and Technological Research Council of Turkey) under Project No.: 113E188.

Author Contributions Contributing to conception and design: SK, BY, AT, OK

Acquiring data, or analyzing and interpreting data: SK, BY, OK, OA, EK, SI

Drafting the manuscript: SK, BY, OK, SI

Critically contributing to or revising the manuscript, or enhancing its intellectual content: SK, BY, EK, SI

Approving the final content of the manuscript: SK, BY, OK

Compliance with Ethical Standards

Conflict of Interest The authors declare that they have no conflict of interest.

References

1. Abe K, Baba S, Kaneko K, Isoda T, Yabuuchi H, Sasaki M, Sakai S, Yoshino I, Honda H: Diagnostic and prognostic values of FDG-PET in patients with non-small cell lung cancer. Clin Imag 33:90–95, 2009
2. Berghmans T, Dusart M, Paesmans M, Hossein-Foucher C, Buvat I, Castaigne C, Scherpereel A, Mascaux C, Moreau M, Roelandts M, Alard S, Meert AP, Patz, Jr EF, Lafitte JJ, Sculier JP, European Lung Cancer Working Party for the IASLC Lung Cancer Staging Project: Primary tumor standardized uptake value (SUVmax) measured on fluorodeoxyglucose positron emission tomography (FDG-PET) is of prognostic value for survival in non-small cell lung cancer (NSCLC): a systematic review and meta-analysis (MA) by

the European Lung Cancer Working Party for the IASLC Lung Cancer Staging Project. J Thorac Oncol 3:6–12, 2008
3. Pugachev A, Ruan S, Carlin S, Larson SM, Campa J, Ling CC, Humm JL: Dependence of FDG uptake on tumor microenvironment. Int J Radiat Oncol 62:545–553, 2005
4. Weber WA, Schwaiger M, Avril N: Quantitative assessment of tumor metabolism using FDG-PET imaging. Nucl Med Biol 27:683–687, 2000
5. van Velden FH, Cheebsumon P, Yaqub M, Smit EF, Hoekstra OS, Lammertsma AA, Boellaard R: Evaluation of a cumulative SUV-volume histogram method for parameterizing heterogeneous intratumoural FDG uptake in non-small cell lung cancer PET studies. Eur J Nucl Med Mol Imaging 38:1636–1647, 2011
6. Chicklore S, Goh V, Siddique M, Roy A, Marsden PK, Cook GJ: Quantifying tumour heterogeneity in 18F-FDG PET/CT imaging by texture analysis. Eur J Nucl Med Mol Imaging 40:133–140, 2013
7. Dong X, Xing L, Wu P, Fu Z, Wan H, Li D, Yin Y, Sun X, Yu J: Three-dimensional positron emission tomography image texture analysis of esophageal squamous cell carcinoma: relationship between tumor 18F-fluorodeoxyglucose uptake heterogeneity, maximum standardized uptake value, and tumor stage. Nucl Med Commun 34:40–46, 2013
8. Orlhac F, Soussan M, Maisonobe J-A, Garcia CA, Vanderlinden B, Buvat I: Tumor texture analysis in 18F-FDG PET: relationships between texture parameters, histogram indices, standardized uptake values, metabolic volumes, and total lesion glycolysis. J Nucl Med 55:414–422, 2014
9. Bagci U, Yao J, Miller-Jaster K, Chen X, Mollura DJ: Predicting future morphological changes of lesions from radiotracer uptake in 18F-FDG-PET images. PloS One 8(2):e57105, 2013
10. Cook GJ, Yip C, Siddique M, Goh V, Chicklore S, Roy A, Marsden P, Ahmad S, Landau D: Are pretreatment 18F-FDG PET tumor textural features in non-small cell lung cancer associated with response and survival after chemoradiotherapy? J Nucl Med 54:19–26, 2013
11. Tixier F, Le Rest CC, Hatt M, Albarghach N, Pradier O, Metges J-P, Corcos L, Visvikis D: Intratumor heterogeneity characterized by textural features on baseline 18F-FDG PET images predicts response to concomitant radiochemotherapy in esophageal cancer. J Nucl Med 52:369–378, 2011
12. Tixier F, Hatt M, Valla C, Fleury V, Lamour C, Ezzouhri S, Ingrand P, Perdrisot R, Visvikis D, Le Rest CC: Visual versus quantitative assessment of intratumor 18F-FDG PET uptake heterogeneity: prognostic value in non–small cell lung cancer. J Nucl Med 55: 1235–1241, 2014
13. Yang F, Thomas MA, Dehdashti F, Grigsby PW: Temporal analysis of intratumoral metabolic heterogeneity characterized by textural features in cervical cancer. Eur J Nucl Med Mol Imaging 40:716–727, 2013
14. Tixier F, Hatt M, Le Rest CC, Le Pogam A, Corcos L, Visvikis D: Reproducibility of tumor uptake heterogeneity characterization through textural feature analysis in 18F-FDG PET. J Nucl Med 53:693–700, 2012
15. Vaidya M, Creach KM, Frye J, Dehdashti F, Bradley JD, El Naqa I: Combined PET/CT image characteristics for radiotherapy tumor response in lung cancer. Radiother Oncol 102:239–245, 2012
16. Soussan M, Orlhac F, Boubaya M, Zelek L, Ziol M, Eder V, Buvat I: Relationship between tumor heterogeneity measured on FDG-PET/CT and pathological prognostic factors in invasive breast cancer. PloS One 9(4):e94017, 2014
17. Ha S, Choi H, Cheon GJ, Kang KW, Chung J-K, Kim EE, Lee DS: Autoclustering of non-small cell lung carcinoma subtypes on 18F-FDG PET using texture analysis: a preliminary result. Nucl Med Mol Imaging 48:278–286, 2014
18. Edge SB, Byrd DR, Compton CC, Fritz AG, Greene FL, Trotti A Eds: AJCC cancer staging manual, 7th edition. New York: Springer, 2010
19. Brooks FJ, Grigsby PW: The effect of small tumor volumes on studies of intratumoral heterogeneity of tracer uptake. J Nuclear Med 55:37–42, 2014
20. Larson SM, Erdi Y, Akhurst T, Mazumdar M, Macapinlac HA, Finn RD, Casilla C, Fazzari M, Srivastava N, Yeung HW, Humm JL, Guillem J, Downey R, Karpeh M, Cohen AE, Ginsberg R: Tumor treatment response based on visual and quantitative changes in global tumor glycolysis using PET-FDG imaging: the visual response score and the change in total lesion glycolysis. Clin Positron Imaging 2:159–171, 1999
21. Otsu N: A threshold selection method from gray-level histograms. Automatica. 11:23–27, 1975
22. Sathya P, Kayalvizhi R: Optimal segmentation of brain MRI based on adaptive bacterial foraging algorithm. Neurocomputing 74: 2299–2313, 2011
23. Wang R, Li C, Wang J, Wei X, Li Y, Zhu Y, Zhang S: Threshold segmentation algorithm for automatic extraction of cerebral vessels from brain magnetic resonance angiography images. J Neurosci Methods 241:30–36, 2015
24. Bashar MK, Komatsu K, Fujimori T, Kobayashi TJ: Automatic extraction of nuclei centroids of mouse embryonic cells from fluorescence microscopy images. PloS one 7(5):e35550, 2012
25. Bagci U, Foster B, Miller-Jaster K, Luna B, Dey B, Bishai WR, Jonsson CB, Jain S, Mollura DJ: A computational pipeline for quantification of pulmonary infections in small animal models using serial PET-CT imaging. EJNMMI Res 3:55, 2013
26. Clausi DA: An analysis of co-occurrence texture statistics as a function of grey level quantization. Can J Remote Sens 28:45–62, 2002
27. Selvarajah S, Kodituwakku S: Analysis and comparison of texture features for content based image retrieval. Int J Latest Trends Computing 2(1):108–113, 2011
28. Haralick RM, Shanmugam K, Dinstein IH: (1973) Textural features for image classification. IEEE Trans Syst Man Cybern Syst 610–21
29. Galloway MM: Texture analysis using gray level run lengths. Comp Vision Graph 4:172–179, 1975
30. Laws KI. Textured image segmentation [Ph.D. thesis] (1980): University of Southern California, Los Angeles
31. Kayaaltı Ö, Aksebzeci BH, Karahan İÖ, Deniz K, Öztürk M, Yılmaz B, Kara S, Asyalı MH: Liver fibrosis staging using CT image texture analysis and soft computing. Appl Soft Comput 25: 399–413, 2014
32. Chu A, Sehgal C, Greenleaf JF: Use of gray value distribution of run lengths for texture analysis. Pattern Recogn Lett 11:415–419, 1990
33. Dasarathy BV, Holder EB: Image characterizations based on joint gray level-run length distributions. Pattern Recogn Lett 12:497–502, 1991
34. Subramanya M, Kumar V, Mukherjee S, Saini M: (2014) A CAD system for B-mode fatty liver ultrasound images using texture features. J Med Eng Technol 1–8
35. Rachidi M, Marchadier A, Gadois C, Lespessailles E, Chappard C, Benhamou C: Laws' masks descriptors applied to bone texture analysis: an innovative and discriminant tool in osteoporosis. Skeletal Radiol 37:541–548, 2008
36. Balagurunathan Y, Kumar V, Gu Y, Kim J, Wang H, Liu Y, Goldgof DB, Hall LO, Korn R, Zhao B, Schwartz LH, Basu S, Eschrich S, Gatenby RA, Gillies RJ: Test–retest reproducibility analysis of lung CT image features. J Digit Imaging 27: 805–823, 2014
37. Tukey JW (1949): Comparing individual means in the analysis of variance. Biometrics 99–114.

38. Benjamini Y, Hochberg: (1995) Controlling the false discovery rate: a practical and powerful approach to multiple testing. J Roy Stat Soc B Met 289–300
39. Miklavčič D, Pavšelj N, Hart FX: Wiley encyclopedia of biomedical engineering. Malden: John Wiley & Sons, Inc, 2006
40. Cortes C, Vapnik V: Support-vector networks. Mach Learn 20:273–297, 1995
41. Pattern PR: Recognition. In: Akay M Ed.. Wiley Encyclopedia of Biomedical Engineering. New York: Wiley, 2006
42. Whitney AW: A direct method of nonparametric measurement selection. IEEE Trans Comput 100:1100–1103, 1971
43. Chierichetti F, Pizzolato G: 18F-FDG-PET/CT. Q J Nucl Med Mol Imag 56:138–150, 2012
44. Vach W, Høilund-Carlsen PF, Gerke O, Weber WA: Generating evidence for clinical benefit of PET/CT in diagnosing cancer patients. J Nucl Med 52:77–85, 2011
45. Castellano G, Bonilha L, Li L, Cendes F: Texture analysis of medical images. Clin Radiol 59:1061–1069, 2004
46. Holli K, Lääperi A-L, Harrison L, Luukkaala T, Toivonen T, Ryymin P, Dastidar P, Soimakallio S, Eskola H: Characterization of breast cancer types by texture analysis of magnetic resonance images. Acad Radiol 17:135–141, 2010
47. Davnall F, Yip CS, Ljungqvist G, Selmi M, Ng F, Sanghera B, Ganeshan B, Miles KA, Cook GJ, Goh V: Assessment of tumor heterogeneity: an emerging imaging tool for clinical practice? Insights Imaging 3:573–589, 2012
48. Ba-Ssalamah A, Muin D, Schernthaner R, Kulinna-Cosentini C, Bastati N, Stift J, Gore R, Mayerhoefer ME: Texture-based classification of different gastric tumors at contrast-enhanced CT. Eur J Radiol 82:537–543, 2013
49. Cheng N-M, Fang Y-HD, Yen T-C: The promise and limits of PET texture analysis. Ann Nucl Med 27:867–869, 2013
50. van Gómez López O, Vicente AMG, Martınez AFH, Soriano AM, Castrejón GAJL, Udias JM, León Atance P: Heterogeneity in [18 F] fluorodeoxyglucose positron emission tomography/computed tomography of non-small cell lung carcinoma and its relationship to metabolic parameters and pathologic staging. Mol Imaging 13:1–12, 2014
51. Sollini M, Cozzi L, Antunovic L, Chiti A, Kirienko M: PET Radiomics in NSCLC: state of the art and a proposal for harmonization of methodology. Sci Rep 7:358, 2017
52. Wu J, Aguilera T, Shultz D, Gudur M, Rubin DL, Loo BW, Diehn M, Li R: (2016) Early-Stage Non–Small Cell Lung Cancer: Quantitative Imaging Characteristics of 18F Fluorodeoxyglucose PET/CT Allow Prediction of Distant Metastasis. Radiology 281(1)
53. Vesselle H, Schmidt RA, Pugsley JM, Li M, Kohlmyer SG, Vallières E, Wood DE: Lung cancer proliferation correlates with [F-18] fluorodeoxyglucose uptake by positron emission tomography. Clin Cancer Res 6:3837–3844, 2000
54. Cawley GC, Talbot NLC: Over-fitting in model selection and subsequent selection bias in performance evaluation. J Machine Learning Research 11:2079–2107, 2010
55. Hatt H, Tixier F, Pierce L, Kinahan PE, Rest CC, Visvikis D: (2016) Characterization of PET/CT images using texture analysis: the past, the present… any future? 44(1):151–165